Ocean acidification and marine trace gas emissions

Frances E. Hopkins[a,b,1], Suzanne M. Turner[a], Philip D. Nightingale[b], Michael Steinke[c], Dorothee Bakker[a], and Peter S. Liss[a]

[a]Laboratory for Global Marine and Atmospheric Chemistry, School of Environmental Sciences, University of East Anglia, Norwich, Norfolk NR4 7TJ, United Kingdom; [b]Plymouth Marine Laboratory, Plymouth, Devon PL1 3DH, United Kingdom; and [c]Department of Biological Sciences, University of Essex, Colchester, Essex CO4 3SQ, United Kingdom

Edited by Michael L. Bender, Princeton University, Princeton, NJ, and approved November 25, 2009 (received for review June 28, 2009)

The oceanic uptake of man-made CO_2 emissions is resulting in a measureable decrease in the pH of the surface oceans, a process which is predicted to have severe consequences for marine biological and biogeochemical processes [Caldeira K, Wickett ME (2003) *Nature* 425:365; The Royal Society (2005) *Policy Document 12/05* (Royal Society, London)]. Here, we describe results showing how a doubling of current atmospheric CO_2 affects the production of a suite of atmospherically important marine trace gases. Two CO_2 treatments were used during a mesocosm CO_2 perturbation experiment in a Norwegian fjord (present day: ~380 ppmv and year 2100: ~750 ppmv), and phytoplankton blooms were stimulated by the addition of nutrients. Seawater trace gas concentrations were monitored over the growth and decline of the blooms, revealing that concentrations of methyl iodide and dimethylsulfide were significantly reduced under high CO_2. Additionally, large reductions in concentrations of other iodocarbons were observed. The response of bromocarbons to high CO_2 was less clear cut. Further research is now required to understand how ocean acidification might impact on global marine trace gas fluxes and how these impacts might feed through to changes in the earth's future climate and atmospheric chemistry.

dimethylsulfide | halocarbons | atmospheric chemistry | climate

Human reliance on the combustion of fossil fuels, combined with activities including deforestation and cement production, has resulted in ever-increasing atmospheric CO_2 concentrations (pCO_2). Current pCO_2 is around 380 μatm—the highest level during the last 650,000 years—and is rising at a rate unprecedented in the Holocene (1–3). The oceans constitute a critical sink for CO_2 and, since the 1980s, have absorbed around 30% of all anthropogenic CO_2 (1, 2). The uptake of this additional CO_2 is resulting in a decrease in the pH of surface waters, manifested as increasing H^+ ion concentrations and decreasing $CaCO_3$ saturation states, an effect widely termed "ocean acidification" (OA) (1–3). The present average surface ocean pH of ~8.1 is 0.1 pH units lower than in preindustrial times, representing a 30% increase in the concentration of H^+ ions (1). Under the Intergovernmental Panel on Climate Change *Special Report on Emissions Scenarios* CO_2 emissions scenarios, atmospheric CO_2 concentrations are predicted to reach between 550 and 1,000 μatm by the year 2100 (4, 5), accompanied by a drop of surface ocean pH of between 0.2 and 0.5 units (1). Such rapid and dramatic changes to ocean carbonate chemistry are argued to have a detrimental impact on marine biota (2, 6).

Iodo- and bromocarbon gases in surface seawater are a major source of halogens to the marine atmosphere, where they are rapidly oxidized to produce reactive radicals. Iodine oxides play a highly significant role in the photochemical loss of tropospheric ozone, a potent oxidant and greenhouse gas (7, 8). Longer-lived halogen species are involved in the natural regulation of the protective layer of stratospheric ozone (9). Additionally, there is direct evidence that iodine oxides can contribute to particle formation (10) and to the production of cloud condensation nuclei in the coastal marine boundary layer, with potentially significant effects on global radiative forcing. Dimethylsulfide (DMS) is also produced in surface seawater and emitted to the atmosphere. Here, it undergoes rapid oxidation to produce particles which, through direct and indirect interactions with incoming solar radiation, affect planetary albedo, with the potential for climate feedbacks (11). Consequently, changes in the production rate and sea-to-air emission of marine trace gases as a result of OA may have significant impacts on atmospheric chemistry and global climate.

We participated in a community mesocosm CO_2 perturbation experiment to study the effect of OA on marine trace gas production. Six mesocosm enclosures (2-m diameter, 3.5-m depth) were deployed in a fjord in Norway, three representing pCO_2 and pH predicted for 2100 (M1, M2, M3 ~750 μatm, pH 7.8) and three acting as present-day controls (M4, M5, M6 ~300 μatm, pH 8.1). CO_2/air mixtures were used to manipulate seawater pH and pCO_2 inside the mesocosms, initially by aeration of the water for 2 days, followed by flushing of the headspace for the remainder of the experiment (Fig. 1 *A* and *B*). Nutrients were added to the mesocosm enclosures on May 6 to stimulate blooms of phytoplankton (final concentrations: 17 μmol l^{-1} nitrate, 1 μmol l^{-1} phosphate; see *Methods* for full details). Seawater samples were collected daily from the enclosures for trace gas analyses. The chlorophyll-*a* data (Fig. 1*C*) shows the evolution of the bloom, and we refer to two phases: May 10 to 17 (bloom), and May 18 to 23 (postbloom).

Results and Discussion

Concentrations of chlorophyll *a* (Fig. 1*C*) began to respond to nutrient addition from May 10, with rapid increases in all enclosures from this point. Maximum concentrations of 6 to 11 mg m^{-3} were attained on May 13 and 14, coinciding with the greatest abundance of microbial plankton, and concentrations were significantly lower under high CO_2 during the bloom phase. Picoeukaryotes dominated the microbial plankton communities, while flagellates were the greatest contributor to the phytoplankton biomass (Figs. S1 and S2). Under high CO_2, numbers of coccolithophores, large picoeukaryotes, cryptophytes, and *Synechococcus* were significantly lower than in the present day CO_2 enclosures (Table S1). Similarly, phytoplankton biomass (g C m^{-3}) was reduced in high CO_2 M1 relative to present CO_2 M6, with a 28% reduction in total biomass, and notable reductions in diatom (81%), autotrophic dinoflagellate (56%), and ciliate biomass (35%) (Table S2). The demise of the bloom began on May 14 and 15, when chlorophyll*a* concentrations began to decline, accompanied by reductions in most components of the microbial plankton community.

The iodocarbon gases (Fig. 1 *D–G*) generally showed similar temporal trends and maximum concentrations were observed during the period of May 14 to 18. Although displaying characteristics associated with biological activity, the iodocarbons do not appear to be directly related to phytoplankton growth, as maximum gas concentrations occurred generally after the maxima in chlorophyll *a*. Furthermore, the timing of initial increases in iodocarbons did not coincide with those of chlorophyll *a* (May 11):

Author contributions: F.E.H., S.M.T., P.D.N., M.S., and P.S.L. designed research; F.E.H. and D.B. performed research; F.E.H. analyzed data; and F.E.H., S.M.T., P.D.N., M.S., and P.S.L. wrote the paper.

The authors delcare no conflict of interest.

This article is a PNAS Direct Submission.

[1]To whom correspondence should be addressed. E-mail: fhop@pml.ac.uk.

This article contains supporting information online at www.pnas.org/cgi/content/full/0907163107/DCSupplemental.

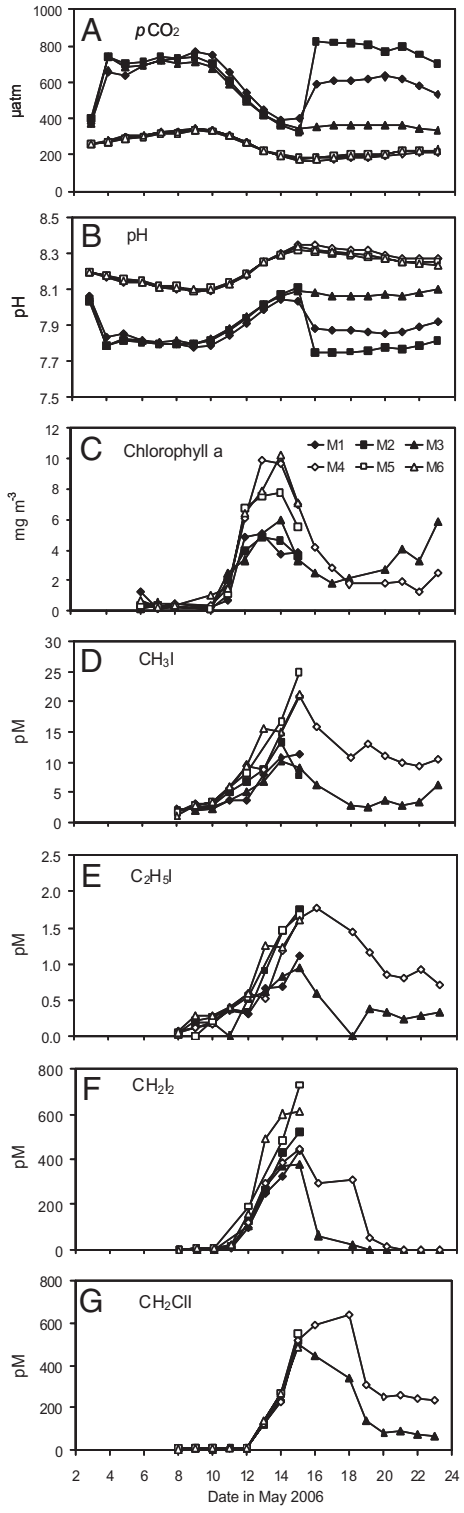

Fig. 1. Temporal changes in pCO_2 (*A*), pH (*B*), chlorophyll *a* (*C*), and the concentrations (pM) of methyl iodide CH_3I (*D*), ethyl iodide C_2H_5I (*E*), diiodomethane CH_2I_2 (*F*), chloroiodomethane CH_2ClI (*G*) over the course of the experiment. Data for M3 and M4 only is shown from May 16 onward as the remaining four mesocosms underwent a second aeration on May 15. Chl *a* concentrations were significantly lower under high CO_2 for the bloom period May 10 to 17 ($T = 2.45$, $P = 0.021$). Significant differences were found for CH_3I for the bloom period ($T = 2.75$, $P = 0.012$). The postbloom period May 18 to 23 saw reductions in all iodocarbons under high CO_2: CH_3I (−67%), C_2H_5I (−73%), CH_2I_2 (−93%), and CH_2ClI (−59%). pH data calculated using TA and pCO_2. See *Tables S1–S5* for details of statistical analyses.

iodomethane (CH_3I) and iodoethane (C_2H_5I) increased from May 8, whereas diiodomethane (CH_2I_2) and chloroiodomethane (CH_2ClI) concentrations began to rise on May 12 and 13, respectively. The data in Fig. 1 strongly suggest that lowered pH leads to a reduction in iodocarbon concentrations. During the bloom phase (May 10–17), the mean concentrations of CH_3I, C_2H_5I and CH_2I_2 were all lower under high CO_2, although only CH_3I showed significant differences ($T = 2.75$, $DF = 22$, $P = 0.012$). Full details of statistical analysis can be found in Tables S3 and S4. There was no difference between treatments for CH_2ClI concentrations during the bloom period. However, during the postbloom phase (May 18–23), all of the iodocarbons exhibited an effect of high CO_2 treatment with average percentage decreases of 67, 73, 93, and 59 for CH_3I, C_2H_5I, CH_2I_2, and CH_2ClI, respectively (Table 1). The differences between treatments were maintained until the end of the experiment, with the exception of CH_2I_2, which returned to its initial concentrations on May 20.

CH_3I and C_2H_5I concentrations under both treatments fell within open-ocean and coastal seawater measurements (12–14), indicating that conditions within the mesocosms were realistic with respect to net production of these gases. C_2H_5I is a minor iodocarbon component of seawater (12), and similarly in this study it made up <1% of the total iodocarbon pool. CH_2I_2 and CH_2ClI concentrations were somewhat elevated compared to most (but not all) oceanic measurements (13, 15) and they dominated the iodocarbon pool, in common with a number of other studies (12, 13, 16). Production of CH_3I is often referred to as "biogenic" (17): directly by macroalgae and phytoplankton (12) and indirectly through a photochemical reaction with organic matter (18). There is little available information on C_2H_5I; however, the present and previous studies have found significant correlations between C_2H_5I and CH_3I, suggesting similar production and removal mechanisms (12, 19, 20) (Fig. S3). CH_2I_2 is considered to have a primarily biogenic source (17). It is subject to rapid photolysis in surface seawater (photolytic lifetime of ∼12 min), with strong evidence that this reaction is an important source of CH_2ClI (21). For the productive mesocosm environment, the processes controlling net iodocarbon production were susceptible to lowered pH. Although chlorophyll-*a* concentrations were lower under high CO_2, the decrease in iodocarbon concentrations was not simply a manifestation of a general decline in biological productivity. This was most apparent during the postbloom phase when iodocarbon-to-chlorophyll-*a* ratios showed large differences between treatments. Mean ratios for CH_3I, C_2H_5I, CH_2I_2 and CH_2ClI to chlorophyll *a* under high CO_2 were 1.1, 0.1, 2.3, and 55.5, respectively, compared to higher values of 5.7, 0.5, 24.7, and 159.9 under present day CO_2. Therefore, despite elevated chlorophyll-*a* concentrations under high CO_2 during the postbloom phase, net production of iodocarbons was greatly reduced. Such changes may be the result of plankton community shifts. Small picoeukaryotes, cryptophytes, and *Synechococcus* were all significantly lower under high CO_2, and the difference between treatments was most pronounced during the postbloom phase (Fig. S1 and Table S1). If any of these organisms are involved in iodocarbon production or consumption, changes in their abundance may directly impact seawater concentrations.

The temporal changes in the concentrations of the bromocarbon gases (Fig. 2 *A–C*) were substantially different to those of the iodocarbons, with large peaks before the development of the bloom, followed by rapid decreases in concentrations. There appeared to be some relationship to biomass over the period of exponential growth. In addition, the bromocarbon concentrations tended to show some increase under high CO_2 (Table 1), and dibromochloromethane ($CHBr_2Cl$) was significantly elevated (bloom 29% increase, $T = -2.82$, $DF = 33$, $P = 0.008$). However, it is not clear whether these differences can be attributed to an effect of pCO_2 and further study is now needed.

Table 1. Summary of trace gas, dimethylsulfoniopropionate, and chlorophyll-*a* data

	Bloom phase May 10–17, all mesocosms			Postbloom phase May 18–23, M3 and M4			Whole experiment May 6–23 (M3 and M4 only after May 15)		
	High CO_2	Present day	% diff.	High CO_2	Present day	% diff.	High CO_2	Present day	% diff.
CH_3I*	6.9	12.1	−43	3.6	10.7	−67	5.4	9.2	−41
C_2H_5I*	0.7	1.0	−32	0.3	1.0	−73	0.5	0.7	−32
CH_2I_2*	197.4	283.4	−30	4.6	63.9	−93	134.6	200.8	−33
CH_2ClI*	189.3	207.2	−9	131.1	321.7	−59	136.9	191.0	−28
$CHBr_3$*	41.2	38.1	+7	14.0	12.1	+14	39.8	34.7	+13
CH_2Br_2*	1.6	1.9	−17	3.29	3.3	+0.3	2.4	2.2	+8
$CHBr_2Cl$*	0.5	0.4	+17	0.7	0.5	+29	0.6	0.5	+22
DMS†	6.1	14.1	−57	15.7	42.0	−63	5.7	14.1	−60
DMSP†	191.7	252.3	−24	182.9	184.3	−0.8	139.0	182.9	−24
Chl a‡	3.2	5.3	−40	3.6	1.8	+49	2.5	3.5	−28

Means and percentage differences of measured variables for high CO_2 treatment and present-day CO_2 treatment for the bloom phase (May 10–17) in all mesocosms, postbloom phase (May 18–23) in M3 and M4, and for the whole experiment.
*pM.
†nM.
‡mg m^{-3}.

Our findings for DMS and its precursor, dimethylsulfoniopropionate (DMSP), are shown in Fig. 3. In all mesocosms, there was an overall increase in DMS concentrations and the temporal trends observed in the two treatments were markedly dissimilar. Under ambient CO_2, both DMS and chlorophyll *a* peaked on May 13 and 14, whereas the high CO_2 DMS displayed only a gentle rise, which did not concur with the trend in chlorophyll *a* (Figs. 1*B* and 3*A*). A large and statistically significant 57% reduction in DMS concentrations was observed under high CO_2 for the bloom period of the experiment ($T = 4.75$, $P < 0.001$) (Table 1). By the end of the experiment, DMS was threefold higher under present day CO_2 compared to the high CO_2 treatment. DMSP concentrations were generally lower under high CO_2 (24%) (Table 1 and Fig. 3B) and displayed significant differences between treatments for the bloom period ($T = 2.18$, $P = 0.038$). DMS and DMSP concentrations are comparable to summertime measurements from nearshore United Kingdom waters (22), and well within the range of measurements during northeast Atlantic coccolithophore blooms (23). This finding provides confirmation of the applicability of mesocosm data to the real world. Our results for DMS are in strong agreement with a mesocosm study in 2004 (24) that showed substantially lower DMS production under high CO_2 (confirmed by a series of in vitro studies). However, the results differ with those from a mesocosm experiment in 2005, which showed only small differences in DMS between elevated and ambient CO_2 treatments (25, 26). The plankton communities of the present study were dominated by flagellates and picoeukaryotes, while the 2005 study was coccolithophore-dominated. It is likely that such differences in community composition may have resulted in the different DMS dynamics seen between the two experiments.

There is considerably more knowledge of the production and removal mechanisms for DMS than for any of the halocarbons. Production of DMS in seawater arises by processes, including active exudation, viral lysis, and grazing by zooplankton, but bacterial consumption is an important removal path (8). These processes act on the phytoplankton cell constituent DMSP, a compound synthesized by a range of phytoplankton species including prymnesiophytes, such as coccolithophores, and dinoflagellates (11). In the communities of the present experiment, these groups of phytoplankton did not dominate [average % total C: prymnesiophytes 16%, dinoflagellates 8%, (Fig S2), coccolithophores 3% of total C, 9% of flagellate biomass (Fig. S4)], thus it is not easy to attribute DMSP production to any particular group of phytoplankton. Because DMSP was less markedly affected by high CO_2, this finding suggests that the change in pH may have

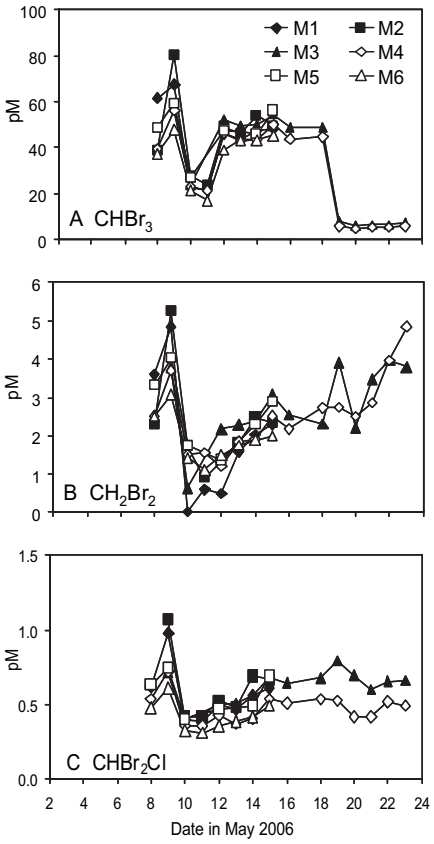

Fig. 2. Temporal changes in the concentrations (pM) of bromoform $CHBr_3$ (*A*), dibromomethane CH_2Br_2 (*B*), and dibromochloromethane $CHBr_2Cl$ (*C*) over the course of the experiment. For the bloom period of May 10 to 17, significant differences were found for $CHBr_2Cl$ ($T = -2.82$, $P = 0.008$). The postbloom period of May 18 to 23 saw increases in $CHBr_3$ (+14%) and $CHBr_2Cl$ (+29%) in the high CO_2 M3, and CH_2Br_2 (+0.3%). See *Tables S1–S5* for details of statistical analyses.

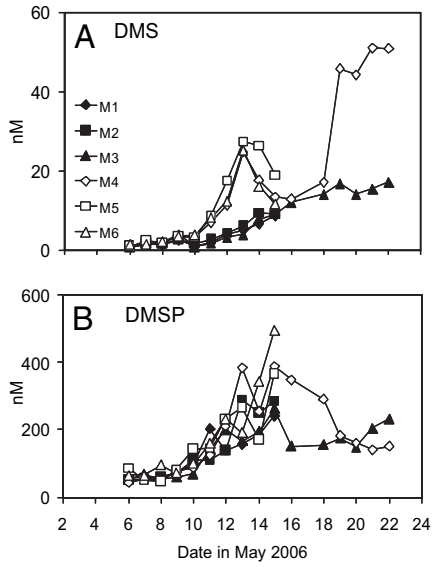

Fig. 3. DMS (*A*) and DMSP(*B*) concentrations (nM) over the course of the experiment. Both DMS and DMSP concentrations for the bloom period of May 10 to 17 were significantly lower under the high CO_2 treatment (DMS T = 4.75, $P < 0.001$; DMSP T = 2.18, $P = 0.038$). The postbloom period of May 18 to 23 saw reductions in DMS (−63%) and DMSP (−0.8%) in the high CO_2 M3 relative to M4. See *Tables S1–S5* for details of statistical analyses.

more impact on the processes that control the conversion of DMSP to DMS rather than the initial production of DMSP itself. Our observed decrease in DMS can be related to climate-model simulations, which show that a 50% decrease in ocean DMS emissions can result in enough net cloud radiative forcing to increase surface air temperature by 1.6°C (27).

Conclusions

Through measurement of realistic concentrations of trace gases during a mesocosm experiment, we have shown that experimentally simulated OA can impact on the production of globally important marine trace gases. Although it would be inappropriate to extrapolate our data to the global oceans, the results of this study are relevant to high productivity areas of the oceans in the high-latitude oceans, coastal waters, and upwelling regions. Not only are these regions of great global importance for the production of biogenic gases, they are expected to experience the greatest changes in terms of anthropogenic ocean acidification and global climate change over the 21st century (5, 28–30).

To assess the impact on global radiative forcing and the atmosphere's oxidative capacity, the complexity of the ocean-atmosphere system must be taken into account. The future ocean will not only be subjected to lowered pH, it will also face physical changes to the climate and ocean system. In combination, all could impact on the sea-to-air flux of trace gases (2, 5). We believe that our findings reveal important effects, and further study is now needed to investigate the response of plankton communities from a range of geographical regions. When incorporated into global ocean-atmosphere modeling studies, information of this kind will be vital to improving prediction of the earth's future climate and atmospheric chemistry.

Methods

The mesocosm experiment was carried out at the Marine Biological Station, Espegrend, Bergen, Norway (Raunefjord, 60.3°N, 5.2°E) from May 3 to 23, 2006. Six reinforced polyethylene enclosures (2-m diameter, 3.5-m depth, 0.5-m above surface of the water) with a total volume 11,000 m^3 were used. The mesocosms were covered with lids consisting of a plastic frame covered in high UV-transmitting horticultural polyethylene, attached to the mesocosms through a system of ropes and karabiners. Although the lids were not intended to be leak-tight, they reduced exchange of the enclosure headspaces with the atmosphere and prevented rain entering. The transmission of photosynthetically active radiation was measured at 92%. The enclosures were attached to the southern side of a raft ≈200-m away from the shore. On May 2, the enclosures were filled with nutrient-deplete, unfiltered water, pumped directly from the fjord. The development of phytoplankton blooms was stimulated by addition of nutrients on May 6 such that initial concentrations in all bags were 1 μmol l^{-1} phosphate and 17 μmol l^{-1} nitrate.

Two treatments were used to assess the effect of high CO_2 on a phytoplankton bloom: "High-CO_2" (M1–M3), and "Present Day" (M4–M6). Water in the high CO_2 enclosures was aerated with ambient air enriched with CO_2 for 1 to 2 days (May 4–6) until pH ~7.8 was attained. From May 6 onwards, the headspaces alone were flushed with high-CO_2 air, thus maintaining the atmospheric concentration and allowing the carbonate system to develop and adjust naturally. The Present Day mesocosms were treated identically, except with the use of ambient air. Discrete samples were collected daily, between 0900 hours and 1000 hours.

Between May 10 and 14, during a period of rapid phytoplankton growth, the pCO_2 gradually decreased back down to near ambient levels, with a concomitant rise in pH (see Fig. 1 *A–C*). Consequently, on May 15, M1 and M2 were reaerated with CO_2 to bring the pH back down to target levels. M3 was left untouched to see what would happen if the experiment had continued unaltered. The present day M4 was also left unaltered, and M5 and M6 were reaerated with air to receive the same physical treatment as M1 and M2. The experiment was continued following this additional treatment until May 23, when sampling ceased.

Mesocosm Sampling. Water sample collection for trace gas analysis was undertaken daily (except May 17 because of technical problems) commencing on May 6 for DMS and May 8 for halocarbons. One sample was taken from all enclosures; triplicate samples were taken from M1 and M6 on alternate days to test analytical reproducibility (Table S5). Water samples for DMS, DMSP, and chlorophyll-*a* analysis were taken with 5-L plastic aspirators. The aspirators were inverted, and then slowly pushed into the water with taps open so that they gently filled up with the least addition of bubbles. A 200-μm mesh was used to cover the opening of the aspirator to exclude large zooplankton and detritus from entering the aspirator. While still on the raft, subsamples were transferred from the aspirators to glass-stoppered bottles using Tygon tubing, which was attached to the tap of the aspirators. To minimize exposure of the water to air during transfer, the tube was placed at the bottom of the bottle. An initial large aliquot was shaken around the bottle to rinse it, and then rejected. Water was then allowed to fill from the bottom of the bottle and sample water was allowed to overflow for an estimated three times the volume of the bottle. The glass-stopper was firmly placed onto the bottle, ensuring the presence of no headspace or bubbles. Each bottle was stored in the dark until all sampling was completed. On return to the onshore laboratory, the samples were kept in a dark, constant-temperature room, maintained at the ambient temperature of the fjord (9–11°C) until analysis.

Samples for halocarbon analyses were taken using 100-mL glass syringes fitted with a syringe extension, consisting of a nylon tube and stopcock. Samples were taken from 20-cm subsurface. Before collection of each sample, ≈50 mL of seawater was drawn up to thoroughly rinse the tubing and syringe, and then rejected. After a second rinse, the sample was gently drawn into the syringe ensuring minimum addition of air bubbles. Immediately after sampling, the glass syringes were placed in a dark box.

Seawater Trace Gas Extraction and Preconcentration. Seawater samples were analyzed similarly to the method of Chuck et al. (14), using purge and trap gas chromatographic systems with flame photometric detector for DMS and mass selective detection (MSD) for halocarbons. Water samples (20 mL for DMS, 40 mL for halocarbons) were analyzed as soon after sample collection as possible, invariably within 2 h of collection. The purge and trap system for DMS was constructed of glass and PTFE, and that for halocarbons of glass and stainless steel. Seawater samples were purged with purified oxygen-free nitrogen at 60 mL min^{-1} for 15 min for DMS, and 40 mL min^{-1} for 20 min for halocarbons. The gases were trapped in a nonpacked sample loop, which was cooled in the headspace of a liquid nitrogen-filled dewar, thermostatically held at −150°C. Analytes were injected onto the GC columns by heating the trap to ~100°C using boiling water.

Halocarbon Analysis. Halocarbon samples were filtered before analysis, through a 47-mm GF/F filter (Whatman) between two syringes, with an inline Swinnex filtration unit. It was ensured that introduction of air was minimized during the process. Once filtered, the sample was injected with 2 μL of the

surrogate analyte mixture and immediately injected into the glass purge vessel of the purge and trap system.

Samples were analyzed using an Agilent gas chromatograph (GC 6890N) and Mass Selective Detector (5975 Series MSD), with a 60-m DB-VRX capillary column installed (0.32 μm film thickness, J & W Ltd.). Following introduction of the samples into the GC, the oven was held at 40°C for 2 min, heated up to 130°C at 8°C min^{-1}, then 200°C at 60°C min^{-1}, and held for 2 min, and finally heated up to 240°C at 60°C min^{-1} and held for a 2 min. The total runtime was 19.08 min, and the data were collected between 3 and 13 min of the run. The MSD was operated in electron ionization (EI)/ single ion mode (SIM) throughout the analyses. To monitor and correct system drift, two surrogate analytes (CD_3I and CD_3CDICD_3) were injected into each sample before analysis. For the compounds with the highest sensitivities (CH_3I and C_2H_5I) CD_3I was used, and CD_3CDICD_3 was used for the compounds with lower sensitivities (CH_2ClI, CH_2I_2, $CHBr_3$, CH_2Br_2, $CHBr_2Cl$). Surrogate analytes were prepared gravimetrically from liquid standards and diluted in HPLC-grade methanol to concentrations of 0.7 pM μL^{-1} CD_3I and 0.9 pM μL^{-1} CD_3CDICD_3. Both surrogate analytes were diluted into one 4-mL amber vial. Immediately before analysis, 2 μL of the surrogate analyte mixture was directly injected into 40-mL seawater samples using a Hamilton constant rate syringe. Calibration and quantification of the compounds was performed using liquid standards prepared in our laboratory. Standards were made up by dilution of the pure compounds into HPLC-grade methanol. The primary standard was prepared gravimetrically, the secondary and working standard by serial dilution. The analytical error for each compound as based on triplicate samples from M1 and M6 were as follows: CH_3I:15%, C_2H_5I:14%, CH_2I_2:15%, CH_2ClI:9%, $CHBr_3$:7%, CH_2Br_2:17%, $CHBr_2Cl$:8%.

DMS and DMSP Analysis. DMS samples were analyzed using a Shimadzu GC-14B with flame photometric detector, with a Shimadzu C-5A Chromatopac integrator. The GC was equipped with a Chromosil 330 (Supelco) packed column, with the oven set at 60°C, the injector set at 150°C, and the detector at 175°C. A 20-mL sample was drawn into a glass gas-tight syringe (20 mL), and slow-filtered through a 25-mm GF/F filter in a Swinnex filtration unit directly into the glass purge vessel for purge and trap analysis. Following injection onto the column, the retention time for DMS was around 1.2 to 1.3 min. Calibration of DMS was performed every 3 to 5 days by cold alkaline hydrolysis of DMSP (31) (0.17–87.6 nM L^{-1}) with 10M NaOH. The analytical error of the system was 6%, as based on triplicate samples from M1 and M6.

For particulate DMSP (DMSP*p*), the filter paper used to filter the DMS sample was placed into a glass vial containing 15 mL of 500 nM NaOH and immediately capped with a crimp seal, cleaving all DMSP to DMS via alkaline hydrolysis. These samples were analyzed for DMSP*p* on return to the United Kingdom by headspace analysis on a Shimadzu GC-2020 with flame photometric detector. Samples of the headspace, ranging from 50 to 250 μL, were taken using a 250-μL Hamilton gas-tight syringe and manually injected into the GC. Calibration of the system was performed using DMSP standard diluted in 500 mM NaOH, in identical 20-mL glass vials, and crimp seals to those used for the samples and over a concentration range of 0.5 to 300 nmol L^{-1}. The analytical error of the system was 11%, based on replicate samples.

***p*CO_2 and pH Determination.** Discrete aqueous samples for the partial pressure of carbon dioxide (*p*CO_2) were taken in 500-mL volumetric flasks from May 3 to 24, 2006. The samples were analyzed within 14 h of collection using a University of East Anglia-built instrument with infrared detection (32). The analysis temperature was within 2°C of the in situ temperature. The CO_2 instrument was calibrated twice daily against secondary standards with CO_2 mixing ratios of 0, 258.40, 470.32, 682.72, and 877.19 μmol mol^{-1}. These secondary standards had been calibrated against National Oceanic and Atmospheric Administration CO_2 standards. The program CO2sys (33), with the equations of Mehrbach et al. (34) as refitted by Dickson and Millero (35), was used to correct for the sample headspace and the temperature difference between sampling and analysis. The pCO_2 was calculated both for the in situ temperature and for a constant temperature of 8°C. The accuracy of pCO_2 is estimated as better than 5 μatm. The average difference between eight replicate samples infers a reproducibility of 3 μatm.

Daily samples for total alkalinity (TA) were taken, filtered, and fixed with mercuric chloride from May 11 to 20. TA was determined by potentiometric titration with a Vindta system at the University of East Anglia. The constants of Prieto and Millero (36) and multiple least-squares fitting were used. Analysis of certified reference material suggests an accuracy and reproducibility of 4 and 2 μmol/kg, respectively. Outliers in TA were replaced by values interpolated from nearby days. TA values for May 3 to 10 have been extrapolated from TA on May 11 and an empirical relationship between TA and coccolithophorid numbers. TA varied little between treatments over this period. pH on the total pH scale was calculated from TA and pCO_2 with CO2SYS (33) with the equations of Mehrbach et al. (34) and Dickson and Millero (35). The variation in calculated pH is dominated by variation in pCO_2, with less effect from changes in TA.

Fig. 1 *A* and *B* show the changes in *p*CO_2 and pH throughout the course of the experiment. On May 3 and 4, the effect of bubbling with CO_2 was clear in M1, M2, and M3 with a rapid increase in *p*CO_2, up to 660 to 736 μatm, accompanied by a sharp drop in pH to 7.8. The rebubbling with CO_2 on May 15 of M1 and M2 is clearly seen as a sharp rise in *p*CO_2, up to 823 μatm, in M2. The pH dropped to 7.9 and 7.7 in M1 and M2, respectively. *p*CO_2 and pH in M3 remained stable for the rest of the experiment, with a mean *p*CO_2 of 358 μatm for this period, and a stable pH of just over 8.1. M3 could still be considered to represent a CO_2-perturbed environment, as *p*CO_2 levels were on average 80 μatm higher than in the Present Day enclosures, a result of the headspace still being flushed with high-CO_2 air. *p*CO_2 in the Present Day mesocosms was on average lower than the fjord itself, with a mean of 250 μatm for the duration of the experiment, compared to 276 μatm for the fjord. This difference arose from higher phytoplankton productivity inside the mesocosms stimulated by the addition of nutrients.

Chlorophyll *a* Determination. Water samples were taken daily from the 5-L aspirators and 350 to 500 mL was filtered through 0.2-μm cellulose acetate filters. The filters were folded four times, placed in a cryovial, and shock-frozen in liquid nitrogen and stored at −80°C until analysis. To extract chlorophyll *a*, filters were placed in 10-mL 90% acetone and left for 24 h at −20°C, then centrifuged at 850 × g for 2 min. Samples were diluted in 90% acetone, with dilution factors of between 5 and 20, and the fluorescence was measured on a Turner Fluorometer. Calibration was performed using chlorophyll-*a* standard diluted in 90% acetone with a concentration range between 1 mg m^{-3} and 20 mg m^{-3}.

Phytoplankton Microscopy Counts. One hundred-milliliter samples from M1 and M6 were preserved with acid Lugol's iodine solution (2% final concentration) and stored in cool, dark conditions until analysis in the laboratory by inverted settlement microscopy (37). Fifty-milliliter subsamples were concentrated by sedimentation for > 24 h and all cells between 2 and 200 μm were enumerated at ×200 or ×400 magnification. Cells were identified, where possible, to species level and their linear dimensions were measured using an ocular micrometer. Cell volumes were calculated using simple geometric shapes and converted to carbon according to the equations of Menden-Deuer and Lessard (38).

Analytical Flow Cytometry. Samples were fixed with 1% paraformaldehyde and used to enumerate microbial plankton using flow cytometry. *Synechococcus*, *Prochlorococcus*, and algae were enumerated in unstained samples with a FACSort flow cytometer (Becton Dickinson) using their specific chlorophyll/phycoerythrin autofluorescence (39). Abundance of heterotrophic bacteria was determined after staining with SYBR Green I DNA dye (40, 41). Yellow-green beads of 0.5-μm diameter (Fluoesbrite Microparticles; Polysciences) were used in all analyses as an internal standard for both fluorescence and flow rates (42). Coccolithophore cell volumes were calculated using simple geometric shapes and converted to carbon (mg C m^{-3}) according to the equations of Menden-Deuer and Lessard (38).

Statistical Analyses. All trace gas, DMSP, and chlorophyll-*a* data were analyzed using two-sample tests of hypotheses. Initially, tests of normality were applied, and if data failed to fit the assumptions of the test, square root transformations of the data were performed. The analysis culminated in a two-sample *t* test. For those data which still failed to display normality following square root transformation, nonparametric tests were applied. Summaries of statistical analyses can be found in *Tables S1–S5*.

ACKNOWLEDGMENTS. We thank all who contributed to the Bergen Mesocosm Experiment, May 2006, particularly I. Mary for the flow cytometry analyses, C. Widdicombe for phytoplankton microscopy counts, K. Crawfurd for total alkalinity sample preparation, G. Lee for his technical support, and M. Liddicoat for help setting up the CO_2 aeration system. Finally, thanks to I. Joint for his leadership of the mesocosm experiment and to all others involved. This work was funded by the Natural Environment Research Council (NERC) NER/S/A/2005/13686 through a CASE PhD studentship between the University of East Anglia and Plymouth Marine Laboratory, Oceans 2025 (P.M.L.'s NERC-funded core program), and the Leverhulme Trust F/00 204/AC.

1. Caldeira K, Wickett ME (2003) Anthropogenic carbon and ocean pH. *Nature* 425:365.
2. The Royal Society (2005) *Ocean acidification due to increasing atmospheric carbon dioxide. Policy Document 12/05* (Royal Society, London).
3. Siegenthaler U, et al. (2005) Stable carbon cycle-climate relationship during the Late Pleistocene. *Science* 310:1313–1317.
4. Nakicenovic N, et al. (2000) *Special Report on Emissions Scenarios* (Intergovernmental Panel on Climate Change) Cambridge University Press, Cambridge, UK and New York, NY.
5. Intergovernmental Panel on Climate Change (2007) Summary for Policymakers. *Climate Change 2007: The Physical Sciences Basis. Working Group I Contribution to the Fourth Assessment Report of the IPCC*, eds Solomon S, et al. (Cambridge Univ. Press, Cambridge).
6. Hall-Spencer JM, et al. (2008) Volcanic carbon dioxide vents show ecosystem effects of ocean acidification. *Nature* 454:96–99.
7. Butler JH, et al. (2007) Oceanic distributions and emissions of short-lived halocarbons. *Global Biogeochem Cycles*, 21:GB1023 10.1029/2006GB002732.
8. Read KA, et al. (2008) Extensive halogen-mediated ozone destruction over the tropical Atlantic Ocean. *Nature* 453:1232–1235.
9. Solomon S, Garcia RR, Ravishankara AR (1994) On the role of iodine in ozone depletion. *J Geophys Res* 99 (D10):20491–20499.
10. O'Dowd C, et al. (2002) Marine aerosol formation from biogenic iodine emissions. *Nature* 417:632–636.
11. Liss PS, Hatton AD, Malin G, Nightingale PD, Turner SM (1997) Marine sulphur emissions. *Philos Trans R Soc Lond, B* 352:159–169.
12. Archer S, Goldson LE, Liddicoat MI, Cummings DG, Nightingale PD (2007) Marked seasonality in the concentrations and sea-to-air flux of volatile iodocarbons compounds in the Western English Channel. *J Geophys Res*, 112:C08009 10.1029/2006JC003963.
13. Abrahamsson K, Lorén A, Wulff A, Wängberg S-A (2004) Air-sea exchange of halocarbons: the influence of diurnal and regional variations and distribution of pigments. *Deep-Sea Res II* 51:2789–2805.
14. Chuck AL, Turner SM, Liss PS (2005) Oceanic distributions and air-sea fluxes of biogenic halocarbons in the open ocean. *J Geophys Res*, 110:C1002 10.1029/2004JC002741.
15. Klick S (1992) Biogenic volatile iodated hydrocarbons in the ocean. *Limnol Oceanogr* 37:1579–1585.
16. Carpenter LJ, Wevill DJ, Palmer CJ, Michels J (2007) Depth profiles of volatile iodine and bromine-containing halocarbons in coastal Antarctic waters. *Mar Chem* 103: 227–236.
17. Moore RM, Zafiriou OC (1994) Photochemical production of methyl iodide in seawater. *J Geophys Res* 99 (D8):16415–16420.
18. Laturnus F (1995) Release of volatile halogenated organic compounds by unialgal cultures of polar macroalgae. *Chemosphere* 31:3387–3395.
19. Mäkelä JM, et al. (2002) Biogenic iodine emissions and identification of end-products in coastal ultrafine particles during nucleation bursts. *J Geophys Res* 107(D19):1.1029/2001JD000580.
20. Richter U, Wallace DWR (2004) Production of methyl iodide in the tropical Atlantic Ocean. *Geophys Res Lett* 31:L23S03 10.1029/2004GL020779.
21. Martino M, Liss PS, Plane JMC (2005) The photolysis of dihalomathanes in surface seawater. *Environ Sci Technol* 39:7097–7101.
22. Turner S, Malin G, Liss PS, Harbour DS, Holligan PM (1988) The seasonal variation of dimethyl sulfide and dimethylsulfoniopropionate concentrations in nearshore waters. *Limnol Oceanogr* 33:364–375.
23. Malin G, Turner S, Liss PS, Holligan PM, Harbour DS (1993) Dimethylsulphide and dimethylsulphoniopropionate in the Northeast Atlantic during the summer coccolithophore bloom. *Deep-Sea Res I* 40:1487–1508.
24. Avgoustidi V (2007) Dimethyl sulphide production in a high-CO2 world. *PhD thesis* (University of East Anglia, Norwich, United Kingdom).
25. Vogt M, et al. (2008) Dynamics of dimethylsulphoniopropionate and dimethylsulphide under different CO_2 concentrations during a mesocosm experiment. *Biogeosciences* 5: 407–419.
26. Wingenter OW, et al. (2007) Unexpected consequences of increasing CO_2 and ocean acidity on marine production of DMS and CH_2ClI: Potential climate impacts. *Geophys Res Lett*, 34 (L05710): 10.1029/2006GL028139.
27. Gunson JR, et al. (2006) Climate sensitivity to ocean dimethylsulphide emissions. *Geophys Res Lett*, 33 (L08801): 10.1029/2005GL024982.
28. Doney SC, et al. (2007) Impact of anthropogenic atmospheric nitrogen and sulphur on ocean acidification and the inorganic carbon system. *Proc Natl Acad Sci USA* 104: 14580–14585.
29. Feely RA, Sabine CL, Hernandez-Ayon JM, Ianson D, Hales B (2008) Evidence for upwelling of corrosive "acidified" water onto the continental shelf. *Science* 320: 1490–1492.
30. Orr JC, et al. (2005) Anthropogenic ocean acidification over the twenty-first century and its impact on calcifying organisms. *Nature* 437:681–686.
31. Turner SM, Malin G, Badanger LE, Leck C (1990) Interlaboratory calibration and sample analysis of dimethyl sulphide in water. *Mar Chem* 29:47–62.
32. Wannikhof RH, Thoning K (1993) Measurement of fugacity of CO_2 in surface water using continuous and discrete sampling methods. *Mar Chem* 44:183–204.
33. Lewis E, Wallace D (1998) Program developed for CO2 systems calculations. ORNL/CDIAC report 105 http://cdiac.esd.ornl.gov/oceans/pubs.html. Accessed June, 2006.
34. Mehrbach C, Culberson CH, Hawley JE, Pytkowiczet RM (1973) Measurement of the apparent dissociation constants of carbonic acid in seawater at atmospheric pressure. *Limnol Oceanogr* 18:897–907.
35. Dickson AG, Millero FJ (1987) A comparison of the equilibrium constants for the dissociation of carbonic acid in seawater media. *Deep-Sea Res* 34:1733–1743.
36. Prieto FJ, Millero FJ (2002) The values of pK1 + pK2 for the dissociation of carbonic acid in seawater. *Geochim Cosmochim Acta* 66:2529–2540.
37. Utermöhl H (1958) Zur Vervollkommnung der quantitativen Phytoplankton Methodik (To the improvement of quantitative phytoplankton methodology). *Mitt Int Verein Theor Angew Limno*, (Communications of the International Association of Theoretical and Applied Limnology) 9:1–38.
38. Menden-Deuer S, Lessard J (2000) Carbon to volume relationships for dinoflagellates, diatoms, and other protist plankton. *Limnol Oceanogr* 45:569–579.
39. Olsen RJ, Zettler ER, DuRand MD (1993) *Handbook of Methods in Aquatic Microbial Ecology*, ed Kemp PF (Lewis Publishers, Boca Raton, FL), pp 175–186.
40. Marie D, Partensky F, Jacquet S, Vaulot D (1997) Enumeration and cell cycle analysis of natural populations of marine picoplankton by flow cytometry using the nucleic acid stain SYBR Green I. *Appl Environ Microbiol* 63:186–193.
41. Zubkov MV, Sleigh MA, Burkill PH, Leakey RJG (2000) Picoplankton community structure on the Atlantic Meridional Transect: a comparison between seasons. *Prog Oceanogr* 45:369–386.
42. Zubkov MV, Fuchs BM, Tarran GA, Burkill PH, Amannet R (2002) Mesoscale distribution of dominant bacterioplankton groups in the northern North Sea in early summer. *Aquat Microb Ecol* 29:135–144.